Defect Spirograph: Dynamical Behavior of Defects in Spatially Patterned Active Nematics

Ali Mozaffari[®], ^{1,*} Rui Zhang, ^{1,2,*} Noe Atzin[®], ¹ and Juan J. de Pablo^{1,3,†}

¹ Pritzker School of Molecular Engineering, The University of Chicago, Chicago, Illinois 60637, USA

² Department of Physics, Hong Kong University of Science and Technology, Clear Water Bay, Kowloon, Hong Kong

³ Center for Molecular Engineering, Argonne National Laboratory, Lemont, Illinois 60439, USA

(Received 28 April 2020; revised 6 January 2021; accepted 3 May 2021; published 2 June 2021)

Topological defects in active liquid crystals can be confined by introducing gradients of activity. Here, we examine the dynamical behavior of two defects confined by a sharp gradient of activity that separates an active circular region and a surrounding passive nematic material. Continuum simulations are used to explain how the interplay among energy injection into the system, hydrodynamic interactions, and frictional forces governs the dynamics of topologically required self-propelling $\pm 1/2$ defects. Our findings are rationalized in terms of a phase diagram for the dynamical response of defects in terms of activity and frictional damping strength. Different regions of the underlying phase diagram correspond to distinct dynamical modes, namely immobile defects, steady rotation of defects, bouncing defects, dancing defects, and multiple defects with irregular dynamics. These dynamic states raise the prospect of generating synchronized defect arrays for microfluidic applications.

DOI: 10.1103/PhysRevLett.126.227801

Active nematics represent a class of nonequilibrium active systems with broken rotational symmetry, where orientational ordering, elastic stresses, active stresses, and hydrodynamic forces interact to produce unique structures and dynamical behaviors [1–7]. Active nematics have drawn considerable interest, and a general understanding of their behavior has begun to emerge from observations across a wide range of experimental systems that include in vitro assemblies of filamentous proteins [8-11], dense suspensions of elongated bacteria [12,13], living nematics [14], and dense colonies of elongated cellular tissues [15–18]. These experiments have been accompanied by theoretical studies that have sought to explain or anticipate their properties [19-33]. In active nematics, active stresses lead to a constant generation and annihilation of topological defects, giving rise to a loss of long-range nematic ordering. The flows associated with these defects are devoid of any spatiotemporal coherence; even for initially ordered systems, regular dynamics and pattern formation are transient [34,35]. Attempts to control and design active nematics are still in their infancy, and have been hindered by a limited understanding of the underlying coupling between structure and dynamics.

Several reports have shown that geometrical confinement and the topological features can be used to stabilize the chaotic motion of active units and to harness their energy to generate well-defined flows [9,36–45]. For example, theory predicts the formation of a circulating pair of $\pm 1/2$ defects under circular confinement, with the bulk dynamics insensitive to the imposed anchoring condition [46]. In unconfined systems, strategies such as assembling extracts of cytoskeletal filaments and motor proteins on anisotropic

soft structured interfaces [47,48], or such as fixing the underlying nematic in contact with a bacterial suspension through a photopatterning [49–51], have both been shown to tame the otherwise chaotic flows. Past work has also sought to harness these flows by relying on frictional forces [36,52–55]. Very recently, the patterning of activity has been shown to be effective at trapping and segregating topological charges, thereby providing a means to guide defect motion [56–58].

In this work, we rely on the relatively new concept of activity patterning or localization, along with the frictional damping, to control defect dynamics in a quasi 2D active nematic. Through this strategy, it becomes possible to confine and further manipulate the dynamics of two, like-charge +1/2 topological defects [Fig. 1(b)]. These new dynamics should be contrasted with those observed for two defects confined by standard hard walls, where momentum cannot be transferred across the boundary, leading to different outcomes and a more limited set of behaviors.

The spatiotemporal evolution of nematic tensorial order parameter ${\bf Q}$ and a flow field ${\bf u}$ follow the continuum equation of motion for an active nematic and are solved using a hybrid lattice Boltzmann method [21,37,59,60]. The details of simulations and the full governing equations are provided in Supplemental Material [61]. Simulations were performed on a 2D lattice confined in a solid disk, with the homeotropic anchoring and no-slip velocity field were enforced at the boundary. The system was initialized with the director field radially oriented. The regions inside the circular domain within the disk were activated by applying uniform extensile active stresses ${\bf \Pi}^a = -\zeta {\bf Q}$, with

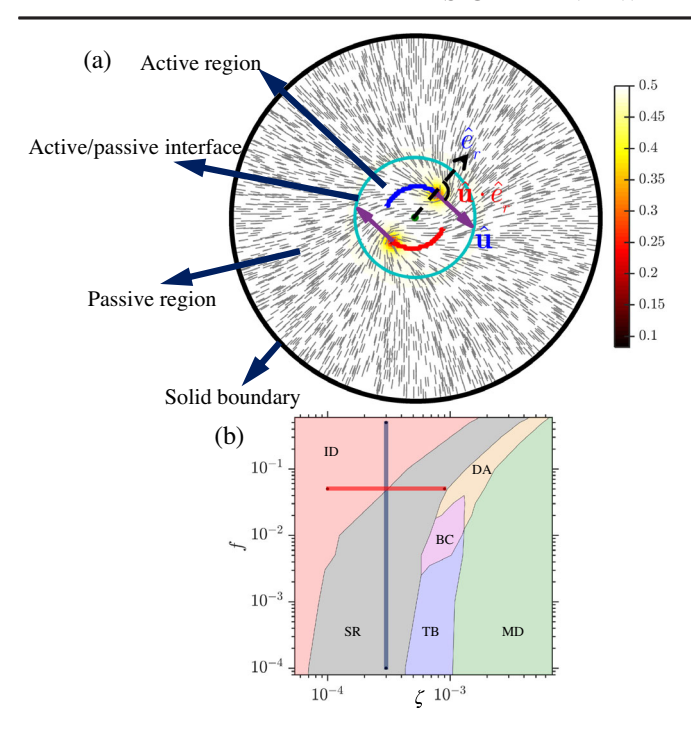


FIG. 1. (a) An snapshot of defect trajectories within the activated region of nematic confined in a solid disk. Purple arrows show the orientation of +1/2 defects (\hat{u}) . The color coding corresponds to the nematic ordering (S). (b) A phase diagram of defect dynamics as a function of activity and friction coefficients.

the activity strength $\zeta > 0$. The domain outside the activated region is passive [Fig. 1(a)].

The Poincaré-Hopf theorem [62] enforces the presence of topological defects of total charge +1 in the current system. As such, the system will develop at least one pair of +1/2 defects, which in the absence of activity experience repulsive interactions that maximize their separation distance. At the same time, the interface created by the spatially inhomogeneous activity profile repels the defects, leading to their entrapment within the active region and the appearance of new patterns and spatiotemporal states (see Supplemental Material and Fig. S1 [61] for a discussion of the repulsive interaction between defects and soft activity interface).

At high values of activity, a transition occurs into a chaotic state, with a fluctuating number of defects, irregular dynamics, continuous formation of bands and their unzipping, and an absence of long-lived defects due to constant defect renovation. As the friction increases, the threshold of activity required for the transition to the multiple defects (MD) with irregular dynamics state becomes larger. The MD state develops when the activity-induced length scale $\sqrt{L/\zeta}$ is smaller than the frictional screening length $\sqrt{\eta/f}$ and the radius of the active circle R, where L is the elastic constant, η is the medium viscosity, and f the friction coefficient.

In passive systems, the free energy is minimized by the formation of two +1/2 defects close to the boundary [63],

whose separation distance is determined by the ratio of the surface anchoring strength and the material's elastic constant. For very low values of activity or for high frictional damping, the active system under consideration behaves as a passive nematic in that it shows two static +1/2 defects facing head to head. In contrast to the behavior of a passive system, however, in the immobile defects (ID) state the stationary defects' separation depends on the relative strength of activity and friction. Note that, as the hydrodynamic screening through frictional forces increases and the system further approaches the dry limit, the defects are pushed further apart and the ID state occupies larger regions of the phase space.

Increasing activity leads to a decrease of the defect separation, as depicted in Fig. 2(a). The self-induced flows of the defects for $\pm 1/2$ defects confined into the solid disk are illustrated in Supplemental Material, Fig. S5 [61]; one

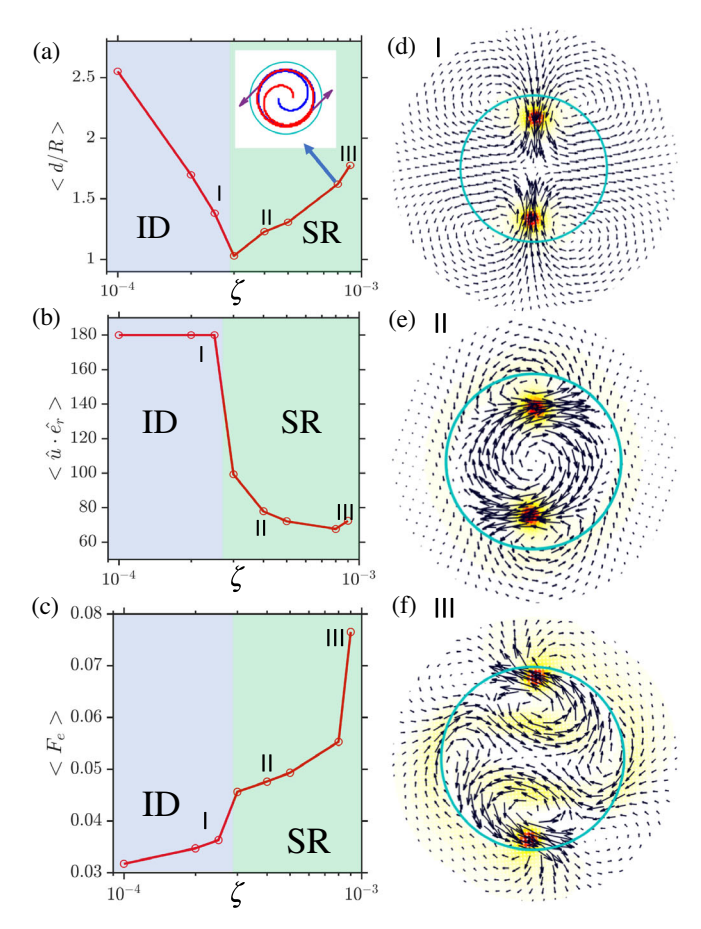


FIG. 2. The effect of activity variation on (a) normalized defect separation, (b) average angle of the defect orientation with the radial vector, and (c) average elastic free energy of the system, for ID and SR states. Points are sampled from the red line in Figs. 1(b), 1(d)–1(f), Velocity field in the domain corresponding to the points marked with I–III. The background color represents the nematic scalar order parameter (S); for the color scale refer to Fig. 1(a). Sample trajectory of two steadily orbiting defects are shown in the inset of Fig. 2(a) ($\zeta = 0.0008$, f = 0.05).

can appreciate a polar double vortex structure for positive charge defects, which drives a cometlike defect toward its head [24]. In the ID state the director field is static. The active stresses, however, generate four equal-sized vortices of deformed quadrupolar structure with a stagnation point in the centroid [Fig. 2(d)]. Increasing activity pushes the defects toward each other, while elastic, friction, and viscous forces keep them apart; all of these forces cancel each other, leading to a static defects state. Note that, despite the defects' lack of motion, active flows are strongest at the defects' core and, consequently, viscous forces are imposed that oppose defect movement.

For a given value of friction, above a critical value of activity, the balance between the forces on the defects is broken. Strong elastic repulsions between +1/2 defects become dominant, and the active forces are unable to bring the defects closer to each other. The defects tilt away from their line of centers [Fig. 2(b)], and enter a persistent circulation with random direction of orbiting, based on spontaneous symmetry breaking [see the inset of Fig. 2(a) for a representative trajectory of steady rotation (SR) of defects, and Supplemental Material, Movie 1 [61]]. In contrast to the behavior of defects confined by hard and impermeable walls, the transition to circulatory motion does not require the creation of an additional pair of defects [46]. The ease of reorientation of the director field at the soft activity boundary allows the system to adapt to the defects' director far field and their underlying advective flows; circumventing the creation of a pair of new defects, giving rise to a smooth transition from ID to SR. Transitions from quiescence into a moving state [37,64–66], and the emergence of coherent circular motion [67,68], are ubiquitous in active matter. Here, we have identified an additional lever for control by showing that the right combination of activity level and friction can be used to tune the precise location of the orbiting; it can be positioned, for example, right at the activity interface [Fig. 3(d)]. Two of the four vortices in the ID state merge to form a larger vortex in the active region, with two additional vortices farther away [Fig. 2(e)].

In the SR state, increasing activity not only drives the defects to orbits having a larger radius (by a stretching of the middle vortex to reduce the high shear) but, due to the enhanced repulsion between them, they adopt an orientation along the radial vector, trying to escape the active region. In contrast, increasing the friction allows the defects to rotate with a smaller orbiting radius, due to the suppression of momentum propagation, the appearance of localized flows, and a reduction of the effective interaction between defects [Fig. 3(a) and Supplemental Material, Fig. S6 [61]].

Figure 3 illustrates the role of friction for a constant value of the activity. For low values of friction, where the defects' orbit is near the activity interface [Fig. 3(d) and Supplemental Material, Movie 2 [61]], the active forces

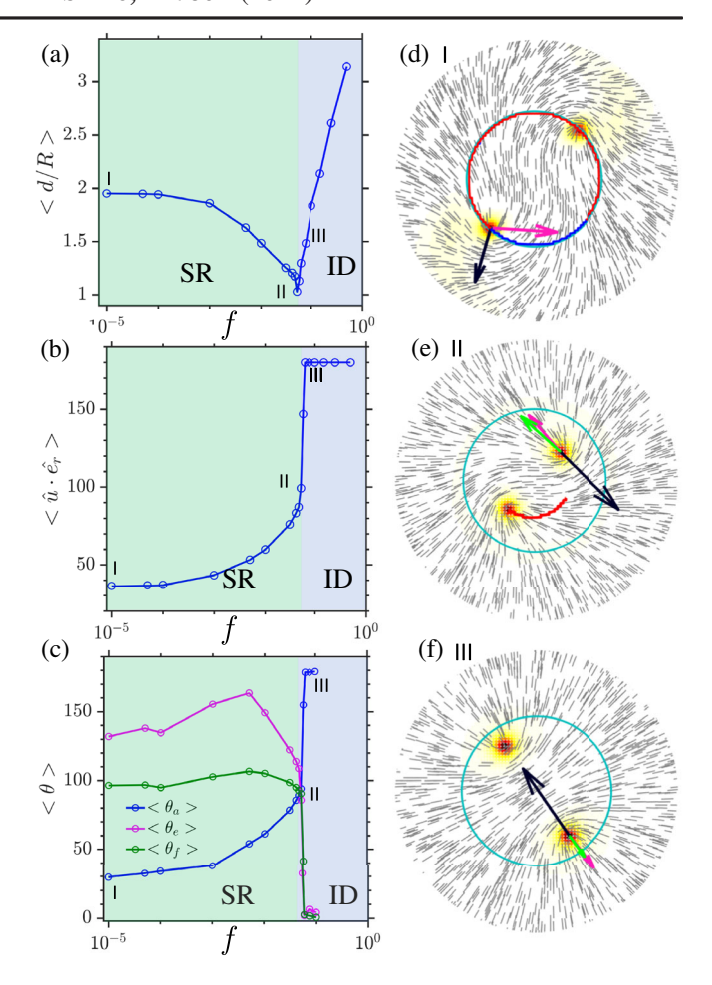


FIG. 3. Effect of friction on ID and SR states. (a) Defect separation normalized by R, (b) average angle between the defect orientation and the radial vector, (c) average of the angles that the active, elastic, and friction forces exerted on the defects make with the radial vector; $\langle \theta_a \rangle$, $\langle \theta_e \rangle$, $\langle \theta_f \rangle$, respectively. Points are sampled from the blue line in Fig. 1(b). (d)–(f) Director field and the trajectories of the defects corresponding to the points marked with I–III. Active, elastic, and frictional forces are denoted by black, pink, and green arrows, respectively. Panels (d),(e) correspond to the SR, where defects orbit in circles and, after the completion of each circle, retrace their steps. Only a part of the circular trajectories is plotted. Elastic and frictional forces in (e),(f) have been magnified by a factor of 2.

are closely oriented along the radial vector \hat{e}_r , while the elastic forces form obtuse angles with the radial vector, keeping the defects inside the active region. As the friction increases, these forces adopt a perpendicular orientation with respect to the radial vector [Figs. 3(c), 3(e), and Supplemental Material, Movie 3 [61]] and, for even larger values of friction, the defects become stationary, with forces parallel to the radial vector [Figs. 3(c) and 3(f)]. Interfacial active forces not only confine the defects inside the active region, but also stabilize their sliding along the activity boundary. Defect steering along the interface is also apparent for the case of a flat active-passive boundary (Fig. S2 and detailed discussions in Supplemental Material [61]).

In the SR state, increasing the activity reduces the nematic ordering, leading to an increase of the elastic free energy [Fig. 2(c)]. For sufficiently large values of friction and activity (see transition from II to III in Fig. 2, and Supplemental Material, Movie 4 [61]), two stable elastic bands (walls) appear between two orbiting defects, which move in phase with the defects. High frictional forces not only allow the two bands that are formed to fit in the active region, but also stabilize them, despite their high elastic cost. Frictional forces reduce the shear stresses across the bands and, consequently, they can approach each other, reducing the effectiveness of long-range hydrodynamic interactions [52,53].

Along these bands, a Poiseuille-like flow is generated, leading to the formation of additional vortices [Fig. 2(f)]. If, in this state, the friction is reduced or the activity is further increased, the elastic penalty incurred by the deformation of these bands increases, causing the bands to unzip by creating a pair of defects on each band [see elastic free energy amplification (reduction) during band formation (unzipping) in Supplemental Material, Movie 5(c) [61]]. While the newly liberated +1/2 defects move along the bands to restore the nematic order, new -1/2 defects annihilate the already existing +1/2 defects, and

this cycle continues to form short-lived dancing defects (DA) (Supplemental Material, Movie 5 [61]). However, if the advective flows are large enough (further increasing the activity), band splitting occurs at the interface, where the stresses are highest, and two fast-moving +1/2 defects from each band switch off and annihilate the newly created -1/2 ones. The original +1/2 defects remain alive, forming a long-lived dancing state [Figs. 4(a), 4(b), and Supplemental Material, Movie 6 [61]].

The two bouncing defects (TB) region in the phase diagram occurs for intermediate values of activity and small friction. In this phase, the active forces and the orientation of the defects form an acute angle, with radial vector \hat{e}_r [Figs. 3(b) and 3(c)], trying to escape the active region. Once they reach the active-passive interface, the active forces drop abruptly and induce a large unfavorable director distortion on the passive side. The system's need to minimize elastic distortions creates elastic forces that catapult the defects back to the active region, forming a "yin yang" structure [Figs. 4(g), 4(h), and Supplemental Material, Movie 8 [61]]. For higher values of activity, the elastic distortion at the passive side next to the interface increases, and the catapulting effect is stronger (faster) with a sharper reflection angle [Figs. 4(e), 4(f), and

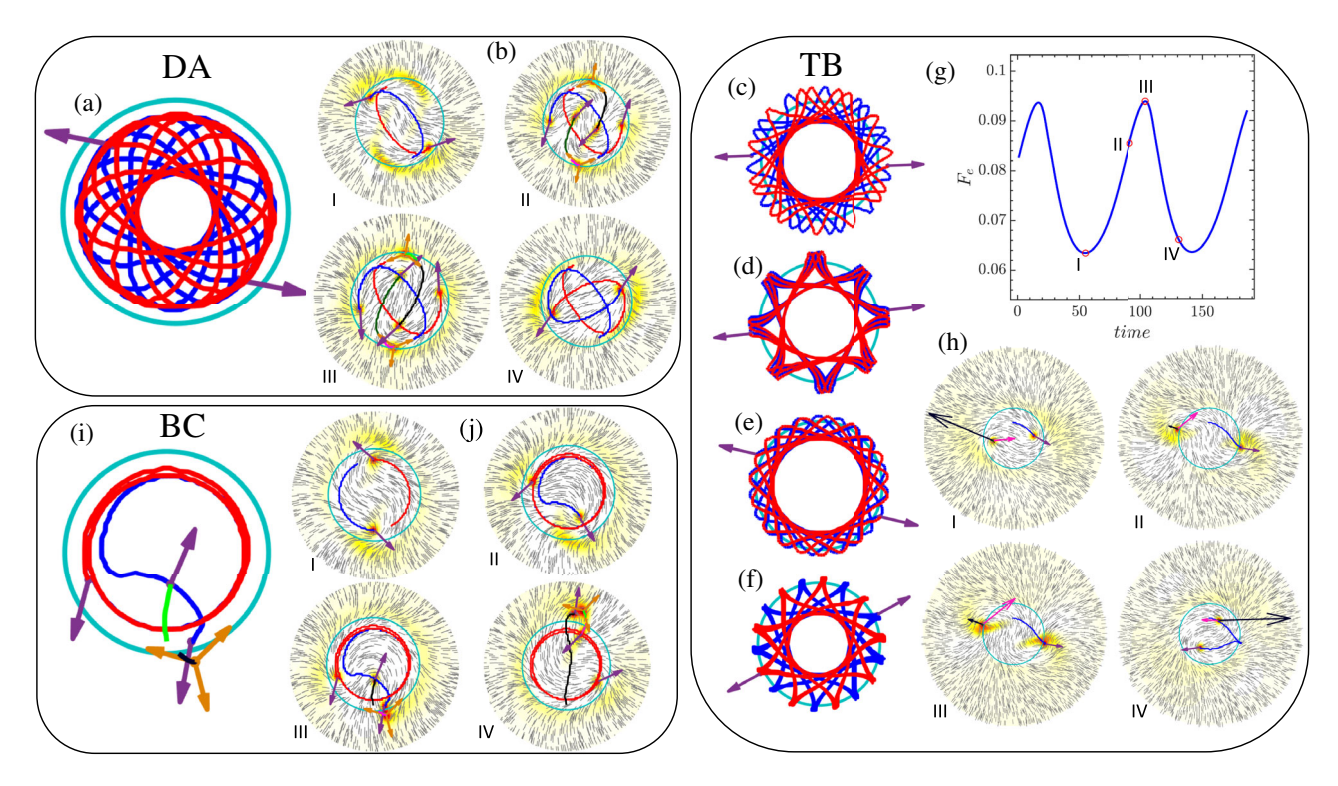


FIG. 4. (a) Defect trajectory, and (b) snapshots of the director field in the dancing state ($\zeta = 0.0016$, f = 0.04). (c)–(f) Long-time defect trajectories for TB state for different values of activity ($\zeta = 0.0005$, 0.0006, 0.0006, 0.0008) and friction (f = 0.0, 0.001, 0.002, 0.002), respectively. Elastic free energy of the system (g) and snapshots of the director with forces exerted on the defect and the defect trajectory (blue) (h); (g),(h) correspond to (f). Active, elastic, and frictional forces are shown with black, pink, and green arrows, respectively (frictional forces are relatively small). (i) Defect trajectories, and (j) snapshots of the director in the BC state ($\zeta = 0.001$, f = 0.01). The orientations of positive (negative) charge defects are identified by purple arrows (a triad of brown arrows). Full blown animations of all of these states are provided in Supplemental Material [61], Movies 5–9.

Supplemental Material, Movie 7 [61]]. An inner, excluded circular region that defects never cross appears, due to strong repulsive interactions. For higher values of activity, where the elastic-rebound effect is sharper, this excluded area becomes smaller (Supplemental Material, Movie 7 [61]).

Two contributions to the active forces, $\mathbf{f}^a = -(\zeta \nabla \cdot \mathbf{Q} + \nabla \zeta \cdot \mathbf{Q})$, arise from (i) the spatial variation of the director field which is most appreciable in the proximity of topological defects and appears in the bulk of the nematic (first term) and, (ii) the large activity gradient $\nabla \zeta$ at the activity interface (second term). The second term, which distinguishes our work from that presented in past studies, is responsible for the rich dynamical states presented here. The direction of this interfacial force depends on the angle between the director field and the activity gradient; note the change of orientation of the force, from radially outward to inward when the director field changes from radial to circular (Fig. S3 [61]). Also, the elastic reorienting torques that the defects exert on each other act to antialign them [27,69], further stabilizing the dynamics of the TB state.

A deeper understanding of the phase diagram can be gained through a theoretical analysis that considers the force and torque balance when one +1/2 defect is near the flat active-passive boundary (Fig. S4 [61]). By balancing the elastic and active contributions to the torque and to the force normal to the boundary, we find that a solution exists when the activity is below a threshold value, which corresponds to the SR state in which defects can glide near the activity boundary. However, if the activity reaches the threshold, a solution no longer exists, indicating that the defect cannot find a steady state near the boundary—in correspondence to the TB state, where defects bounce away as soon as they approach the interface.

We conclude our discussion with a brief mention of a peculiar behavior that we refer to as bouncing-cruising (BC) defects, in which one of the defects undergoes a cruising behavior, and the other shows a bouncing behavior. The viscous forces that drive the long range hydrodynamic interactions, and the frictional forces, compete with each other; the resulting screening length scale $\sqrt{\eta/f}$, defines the width of the elastic bands that form within the active region. Higher values of frictional damping are required to observe the dancing state that is instigated by the pair of oppositely oriented bands; the active region cannot accommodate two bands and, as such, the system develops one band by breaking the symmetry of the flow and the director field. Figures 4(i) and 4(j) show that while one of the defects shows a persistent circular motion, the other one moves toward the interfacial region to induce a radially oriented bending instability. The newly formed band splits and creates a -1/2 defect, which rapidly annihilates the original defect, while the new +1/2 defect is propelled away from the interface (Supplemental Material, Movie 9 [61]). This behavior shares some similarities with the experimental observation of doubly periodic dynamics of defects, obtained from the slow nucleation of defects at the boundary and fast circulating defects in the bulk of microtubule-based active nematics under circular confinement [43]. The creation of -1/2 defects at the solid wall might be indicative of the slippery flow of microtubules at the disk surface, which induces tangential flows that, in turn, drive bending instabilities and creation of a defect pair, similar to the BC state.

We have described a new physical scenario in which the simple spatial patterning of activity leads to defect confinement within a passive-active interface. When coupled to the control of friction at a substrate, we have shown that it becomes possible to program defect motion, thereby turning otherwise chaotic trajectories into precisely sculpted spatiotemporal states and flow fields.

We thank Andrey Sokolov, Alexey Snezhko, Vincenzo Vitelli, and Xingzhou Tang for very helpful discussions. This work on development of a fundamental understanding the structure and dynamics of active nematic liquid crystals is supported by the department of energy, basic energy sciences, division of materials science and engineering. The application of this work to the control of topological defects for logic operations is supported by the National Science Foundation, DMR-2011854. R. Z. also acknowledges the financial support of the Hong Kong RGC under Grant No. 26302320.

These authors contributed equally.

[™]depablo@uchicago.edu

^[1] S. Ramaswamy, Annu. Rev. Condens. Matter Phys. 1, 323 (2010).

^[2] M. C. Marchetti, J.-F. Joanny, S. Ramaswamy, T. B. Liverpool, J. Prost, M. Rao, and R. A. Simha, Rev. Mod. Phys. 85, 1143 (2013).

^[3] D. Needleman and Z. Dogic, Nat. Rev. Mater. 2, 17048 (2017).

^[4] A. Doostmohammadi, J. Ignés-Mullol, J. M. Yeomans, and F. Sagués, Nat. Commun. 9, 3246 (2018).

^[5] M. R. Shaebani, A. Wysocki, R. G. Winkler, G. Gompper, and H. Rieger, Nat. Rev. Phys. 2, 181 (2020).

^[6] J. Ignés-Mullol and F. Sagués, Curr. Opin. Colloid Interface Sci. 49, 16 (2020).

^[7] R. Zhang, A. Mozaffari, and J. J. de Pablo, Nat. Rev. Mater. 6, 437 (2021).

^[8] T. Sanchez, D. T. Chen, S. J. DeCamp, M. Heymann, and Z. Dogic, Nature (London) 491, 431 (2012).

^[9] F. C. Keber, E. Loiseau, T. Sanchez, S. J. DeCamp, L. Giomi, M. J. Bowick, M. C. Marchetti, Z. Dogic, and A. R. Bausch, Science 345, 1135 (2014).

^[10] N. Kumar, R. Zhang, J. J. de Pablo, and M. L. Gardel, Sci. Adv. 4, eaat7779 (2018).

^[11] D. P. Rivas, T. N. Shendruk, R. R. Henry, D. H. Reich, and R. L. Leheny, Soft Matter 16, 9331 (2020).

^[12] J. Dunkel, S. Heidenreich, K. Drescher, H. H. Wensink, M. Bär, and R. E. Goldstein, Phys. Rev. Lett. **110**, 228102 (2013).

- [13] H. Li, X.-q. Shi, M. Huang, X. Chen, M. Xiao, C. Liu, H. Chaté, and H. Zhang, Proc. Natl. Acad. Sci. U.S.A. 116, 777 (2019).
- [14] S. Zhou, A. Sokolov, O. D. Lavrentovich, and I. S. Aranson, Proc. Natl. Acad. Sci. U.S.A. 111, 1265 (2014).
- [15] G. Duclos, C. Erlenkämper, J.-F. Joanny, and P. Silberzan, Nat. Phys. 13, 58 (2017).
- [16] K. Kawaguchi, R. Kageyama, and M. Sano, Nature (London) 545, 327 (2017).
- [17] C. Blanch-Mercader, V. Yashunsky, S. Garcia, G. Duclos, L. Giomi, and P. Silberzan, Phys. Rev. Lett. 120, 208101 (2018).
- [18] D. Dell'Arciprete, M. Blow, A. Brown, F. Farrell, J. S. Lintuvuori, A. McVey, D. Marenduzzo, and W. C. Poon, Nat. Commun. 9, 4190 (2018).
- [19] R. A. Simha and S. Ramaswamy, Phys. Rev. Lett. 89, 058101 (2002).
- [20] V. Narayan, S. Ramaswamy, and N. Menon, Science 317, 105 (2007).
- [21] D. Marenduzzo, E. Orlandini, and J. M. Yeomans, Phys. Rev. Lett. 98, 118102 (2007).
- [22] L. Giomi, L. Mahadevan, B. Chakraborty, and M. F. Hagan, Phys. Rev. Lett. 106, 218101 (2011).
- [23] L. Giomi, M. J. Bowick, X. Ma, and M. C. Marchetti, Phys. Rev. Lett. 110, 228101 (2013).
- [24] L. Giomi, Phys. Rev. X 5, 031003 (2015).
- [25] E. J. Hemingway, P. Mishra, M. C. Marchetti, and S. M. Fielding, Soft Matter 12, 7943 (2016).
- [26] A. Doostmohammadi, S. P. Thampi, and J. M. Yeomans, Phys. Rev. Lett. 117, 048102 (2016).
- [27] S. Shankar, S. Ramaswamy, M. C. Marchetti, and M. J. Bowick, Phys. Rev. Lett. 121, 108002 (2018).
- [28] M. M. Norton, P. Grover, M. F. Hagan, and S. Fraden, Phys. Rev. Lett. 125, 178005 (2020).
- [29] D. Pearce, J. Nambisan, P. Ellis, Z. Dogic, A. Fernandez-Nieves, and L. Giomi, arXiv:2004.13704.
- [30] F. Vafa, M. J. Bowick, M. C. Marchetti, and B. I. Shraiman, arXiv:2007.02947.
- [31] M. Serra, L. Lemma, L. Giomi, Z. Dogic, and L. Mahadevan, arXiv:2104.02196.
- [32] R. Mueller and A. Doostmohammadi, arXiv:2102.05557.
- [33] B. Mahault and H. Chaté, arXiv:2104.05453.
- [34] B. Martínez-Prat, J. Ignés-Mullol, J. Casademunt, and F. Sagués, Nat. Phys. **15**, 362 (2019).
- [35] A. Sokolov, A. Mozaffari, R. Zhang, J. J. de Pablo, and A. Snezhko, Phys. Rev. X 9, 031014 (2019).
- [36] H. Wioland, F. G. Woodhouse, J. Dunkel, J. O. Kessler, and R. E. Goldstein, Phys. Rev. Lett. 110, 268102 (2013).
- [37] M. Ravnik and J. M. Yeomans, Phys. Rev. Lett. 110, 026001 (2013).
- [38] R. Zhang, Y. Zhou, M. Rahimi, and J. J. de Pablo, Nat. Commun. 7, 13483 (2016).
- [39] D. Khoromskaia and G. P. Alexander, New J. Phys. **19**, 103043 (2017).
- [40] K.-T. Wu, J. B. Hishamunda, D. T. Chen, S. J. DeCamp, Y.-W. Chang, A. Fernández-Nieves, S. Fraden, and Z. Dogic, Science 355, eaal1979 (2017).
- [41] P. W. Ellis, D. J. Pearce, Y.-W. Chang, G. Goldsztein, L. Giomi, and A. Fernandez-Nieves, Nat. Phys. 14, 85 (2018).

- [42] P. Guillamat, Ž. Kos, J. Hardoüin, J. Ignés-Mullol, M. Ravnik, and F. Sagués, Sci. Adv. 4, eaao1470 (2018).
- [43] A. Opathalage, M. M. Norton, M. P. Juniper, B. Langeslay, S. A. Aghvami, S. Fraden, and Z. Dogic, Proc. Natl. Acad. Sci. U.S.A. 116, 4788 (2019).
- [44] J. Hardoüin, J. Laurent, T. Lopez-Leon, J. Ignés-Mullol, and F. Sagués, Soft Matter 16, 9230 (2020).
- [45] M. Rajabi, H. Baza, T. Turiv, and O. D. Lavrentovich, Nat. Phys. 17, 260 (2021).
- [46] M. M. Norton, A. Baskaran, A. Opathalage, B. Langeslay, S. Fraden, A. Baskaran, and M. F. Hagan, Phys. Rev. E 97, 012702 (2018).
- [47] P. Guillamat, J. Ignés-Mullol, and F. Sagués, Proc. Natl. Acad. Sci. U.S.A. 113, 5498 (2016).
- [48] P. Guillamat, J. Ignés-Mullol, and F. Sagués, Nat. Commun. 8, 564 (2017).
- [49] C. Peng, T. Turiv, Y. Guo, Q.-H. Wei, and O.D. Lavrentovich, Science 354, 882 (2016).
- [50] T. Turiv, R. Koizumi, K. Thijssen, M. M. Genkin, H. Yu, C. Peng, Q.-H. Wei, J. M. Yeomans, I. S. Aranson, A. Doostmohammadi *et al.*, Nat. Phys. 16, 481 (2020).
- [51] O. D. Lavrentovich, Liq. Cryst. Rev. 1 (2021).
- [52] S. P. Thampi, R. Golestanian, and J. M. Yeomans, Phys. Rev. E 90, 062307 (2014).
- [53] A. Doostmohammadi, M. F. Adamer, S. P. Thampi, and J. M. Yeomans, Nat. Commun. 7, 10557 (2016).
- [54] D. J. G. Pearce, Phys. Rev. Lett. 122, 227801 (2019).
- [55] K. Thijssen, D. Khaladj, S. A. Aghvami, M. A. Gharbi, S. Fraden, J. M. Yeomans, L. S. Hirst, and T. N. Shendruk, arXiv:2102.10184.
- [56] R. Zhang, S. A. Redford, P. V. Ruijgrok, N. Kumar, A. Mozaffari, S. Zemsky, A. R. Dinner, V. Vitelli, Z. Bryant, M. L. Gardel *et al.*, Nat. Mater. (2021), https://doi.org/10.1038/s41563-020-00901-4.
- [57] S. Shankar and M. C. Marchetti, Phys. Rev. X 9, 041047 (2019).
- [58] X. Tang and J. V. Selinger, Phys. Rev. E 103, 022703 (2021).
- [59] R. Zhang, T. Roberts, I. S. Aranson, and J. J. de Pablo, J. Chem. Phys. 144, 084905 (2016).
- [60] R. Zhang, N. Kumar, J. L. Ross, M. L. Gardel, and J. J. de Pablo, Proc. Natl. Acad. Sci. U.S.A. 115, E124 (2018).
- [61] See Supplemental Material at http://link.aps.org/ supplemental/10.1103/PhysRevLett.126.227801 for detailed discussion of the role of active-passive boundary as a soft interface in defect dynamics, simulation details, and movies of defect dynamics.
- [62] R. D. Kamien, Rev. Mod. Phys. 74, 953 (2002).
- [63] V. Vitelli and D. R. Nelson, Phys. Rev. E 70, 051105 (2004).
- [64] R. Voituriez, J.-F. Joanny, and J. Prost, Europhys. Lett. 70, 404 (2005).
- [65] F. G. Woodhouse and R. E. Goldstein, Phys. Rev. Lett. 109, 168105 (2012).
- [66] G. Duclos, C. Blanch-Mercader, V. Yashunsky, G. Salbreux, J.-F. Joanny, J. Prost, and P. Silberzan, Nat. Phys. 14, 728 (2018).
- [67] F. J. Segerer, F. Thüroff, A. P. Alberola, E. Frey, and J. O. Rädler, Phys. Rev. Lett. 114, 228102 (2015).
- [68] S. Liu, S. Shankar, M. C. Marchetti, and Y. Wu, Nature (London) 590, 80 (2021).
- [69] A. J. Vromans and L. Giomi, Soft Matter 12, 6490 (2016).